UDC 551.515.4:551.578.7:551.558.1

Mesoscale Circulations Associated with Alberta Hailstorms

GERD RAGETTE [1]—*Department of Meteorology, McGill University, Montreal, Quebec, Canada*

ABSTRACT—Wind measurements were made near Alberta, Canada, hailstorms during the summers of 1966–68. Pilot balloons were released from a network of ground stations before, during, and after the passage of storms. Out of some 20 cases, five hailstorms were analyzed in detail. The main objective was to study the mesoscale wind pattern associated with the storms from the surface to the highest possible altitude. Patterns of divergence, vorticity, and vertical motion were derived and examined in relation to the radar echoes.

Downward air motions were found in the lower levels throughout most of the horizontal extent of the echoes. In three cases, downdrafts extended downwind of the precipitation; the mesoscale downdraft core was located in the rear portion of the echo with the descending air flowing opposite to the direction of storm motion. In the one case in which downdrafts were confined to the precipitation area, the downdraft core was located in the central part of the echo and the air descended toward the right of the direction of storm motion. Divergence accompanying the downdrafts extended from the surface up to about 4,000 or 5,000 ft and to a higher altitude in the case of a rapidly dissipating storm. A divergence maximum was found in all cases at about 1,000 ft. In general, divergence was associated with anticyclonic vorticity.

Mesoscale updraft areas were observed in some of the cases. A region of ascending air was found on the right flank of a supercell storm. The velocities in this updraft reached 1 m/s at 2,000 ft. The horizontal motion of this ascending region was directed toward an indentation in the echo. In another case, a mesoscale updraft was observed ahead of a squall line. The convergence patterns accompanying the updrafts indicated a low-level convergence maximum at about 1,000 ft in all cases.

In three cases, gust fronts were observed ahead of the storms. They were zones of cyclonic shear closely identified with maxima of cyclonic vorticity and convergence in the updraft region, the effects of which were evident a considerable distance in advance of the gust front. Two different gust front organizations were observed. One seems to be associated with storms that have passed their most active stage. In these cases, the gust front was located several kilometers ahead of the precipitation, and the air pushed ahead of the echo. The other appears to represent an early stage of gust formation, and was associated with a storm still in full vigor. Here, precipitation was encountered ahead of the gust front and the airflow was not directed ahead of the echo, but toward its right-hand side.

1. INTRODUCTION

As part of the Alberta Hail Studies field program in the summers of 1966–68, pilot balloons were released near convective storms by mobile crews. The balloons were tracked optically, sometimes by two theodolites, sometimes by one. Radiosonde ascents occasionally provided additional wind data. These various measurements were used to determine the wind field and the patterns of divergence and vertical motion associated with convective storms.

This paper describes the analysis procedures and illustrates the results for one case. A summary is then given of results for all five cases analyzed. The interested reader may wish to refer to a longer report (Ragette 1971) for more details about the other cases.

2. ANALYSIS METHODS

Wind measurements obtained at different times and different observation sites were combined by assuming that a steady wind field moves with the radar echo pattern. The echo motion was determined by tracing the outline of horizontal plan-position indicator (PPI) echoes at time intervals of about 20 min and employing Thyer's (1970) method of fitting a set of parallel regression lines to the echo trajectory. This amounts to a formal and objective method for obtaining the best-fit, straight line, constant-speed, echo motion over the 20-min period. On the basis of this echo motion, all balloon positions are transformed to fictitious positions relative to the echo at a specified time of interest, thus yielding a quasi-instantaneous picture of the wind field at that time. This kind of time-to-space conversion has been used by Fujita (1955) and many others in mesometeorological studies. It assumes that the wind field moves with the storm but remains relatively unchanged, over the time of observation.

To increase the accuracy of wind measurements, we smoothed the balloon position data using the procedure described by Thyer (1967). The calculations yield the average wind velocity over altitude layers of specified thickness, usually 500, 1,000, or 2,000 ft. The thickness chosen in each case was dictated by the horizontal spacing of balloon observations, their height above ground, the frequency of theodolite readings, and the general quality of the data.

The pattern of divergence was calculated from the wind field using the triangle method (Bellamy 1949). In this method, the separation between observation points affects

[1] Now at the Zentralanstalt für Meteorologie und Geodynamik, A-1190 Wien, Austria

the range over which the calculated divergence values may vary. Triangles with different spacings of the vertices thus yield values that are not strictly comparable. In the present work all the possible triangles for the observational network were classified by size and shape, and only those triangles were used that were approximately isosceles in shape and with areas on the order of 100 mi^2. This selection process reduced the incompatibility of the data and gave a more consistent set of divergence values. Patterns of vorticity were derived using basically the same method.

Vertical velocities were obtained from divergence patterns by integrating the equation of continuity. The local change in density and the horizontal density gradient were neglected. The vertical gradient was approximated using a constant temperature lapse rate and a fixed surface temperature. At the top of an altitude layer, the vertical velocity at the center of each triangle was computed from the mean divergence within the triangle and the vertical velocity at the top of the layer below. This was not strictly a vertical integration since the position, size, and shape of a triangle change as the balloons ascend. Like the divergence values, the vertical velocities thus calculated represent averages over the triangle areas. Though velocities of ± 1 m/s and more were computed, typical values were of the order of 10^{-1} m/s. All computed fields were drawn automatically by digital plotter. An allowance was made for possible overlap of the various triangles used.

To assess the accuracy of single-theodolite winds, we compared the winds obtained by the double-theodolite method with those obtained from one of the theodolites, assuming a constant rate of balloon ascent. A statistical analysis of the data indicated that a 10-percent deviation from the assumed height is likely to occur within the first 20 min after release. The calculated winds in the single-theodolite method may thus be attributed to a wrong level, although the height error has only a small effect on the wind considered as a function of time after release. Only in cases of appreciable downdrafts were single-theodolite pibals found to be too unreliable to be useful.

An error analysis, applied to the calculations of divergence and vertical velocity, showed that the uncertainties arising from observational errors were usually an order of magnitude less than the divergences and vertical velocities measured near storms. More problematic are the inconsistencies and discrepancies arising from the analysis scheme, in particular the steady-state assumption that permits the time-to-space transformation of the observations. To minimize the error from this assumption, the behavior of the radar pattern and the wind observations were examined carefully. For a given storm, a time limit was determined within which the steady-state assumption appeared to be justified. For the cases studied, these time limits varied between 20 and 90 min. Divergence values were then calculated only for those sets of ascent triplets that had no time separation exceeding the predetermined limit. For these computations, the mean wind along a triangle side was assumed to be equal to the arithmetic mean of the winds at the two vertices. This may not be the case when the wind field is nonlinear. The emergence

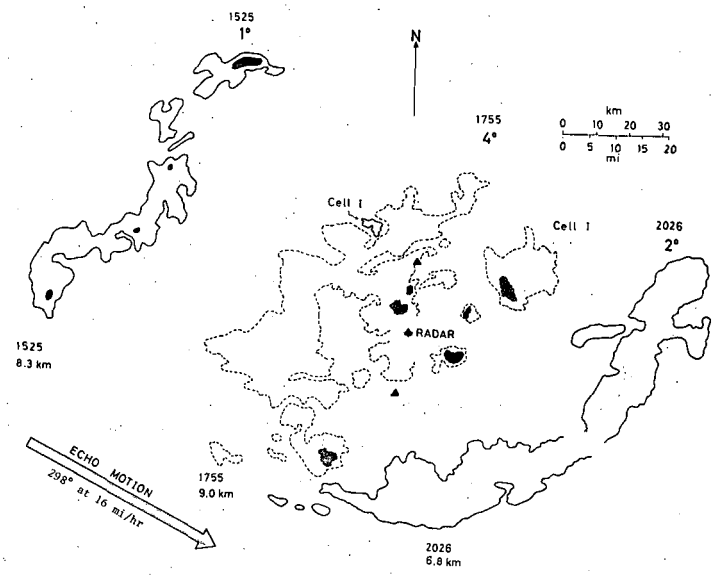

FIGURE 1.—PPI sections at three different times. Outer echo contours indicate gray shade 1 (reflectivity factor of about 10–20 dBZ, depending on range) and dark shading indicates gray shade 4 (about 45 dBZ. Numbers indicate time (MST), antenna elevation angle (°), and height of radar top above the surface (km). Pibal sites are shown by black triangles (radar site included).

of organized patterns in the calculated fields, which are in agreement with results found elsewhere, provides some support for the reliability of the analysis. The case study presented in the next section illustrates the kind of results obtained from the analysis of five Alberta hailstorms.

3. A CASE STUDY—HAILSTORM OF JULY 17, 1968

Echo Pattern and Environment

On July 17, 1968, a large storm system passed over the radar site located at the field headquarters in Penhold, Alberta. The storm lasted for more than 5 hr. At times, its lateral extent exceeded 150 km.

In its early phase, the storm system consisted of two distinct parts, a squall-line type echo complex preceded by a small storm, cell I. Figure 1 illustrates the situation at three different times at 2½-hr intervals. The 1525 MST/1° PPI (i.e., with an antenna elevation angle of 1°) displays the squall line, at this time about 100 km long, consisting of a number of cell swith small reflectivity maxima. Cell I, located 50 km ahead of the squall line, was still in its earliest development. Its radar top was just below 5 km, while tops in the squall line exceeded 8 km. This small leading cell I is 15 km northwest of the northernmost pibal site (fig. 1). The distance between these two echo systems decreased gradually. At 1630 MST, cell I was only 30 km away from the squall line, which spread out in the direction of its motion. The 1755/4° PPI in figure 1 shows cell I still as a separate entity with a top of about 9 km, although it is in the process of being incorporated into the squall-line system, which at this stage of development has spread into a large mass of echo. One-half hour later, cell I had been amalgamated into the storm system, which subsequently began to spread more laterally. It reached

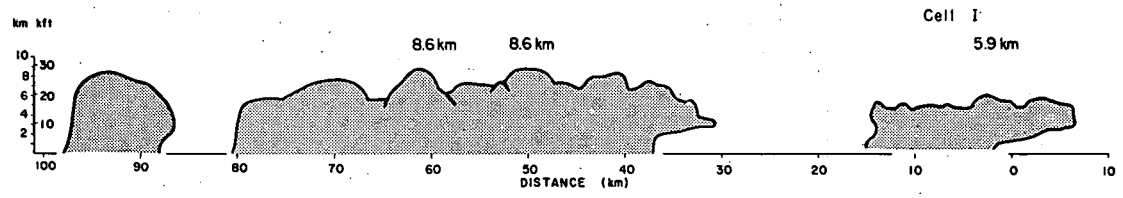

FIGURE 2.—Shaded areas display the projection of echoes at 1637 MST on a vertical plane in the direction of storm motion with horizontal distance measured from the projection of the radar site. Diagram is in true scale.

its maximum lateral extent by about 1930 MST when the 2° PPI indicated a 150-km long echo. The 2026/2° PPI still shows an echo of considerable size, but weak reflectivities, with radar tops around 6 km.

The entire storm system is displayed in figure 2. The radar echo projection was reconstructed from the PPI of 1637 MST by projecting the echo on a vertical plane in the direction of storm motion. The squall line was organized as a line oriented perpendicular to the plane of this figure with several of the peaks shown in the echo outline as much as 100 km apart. The separate echo at the rear and the one peak on the left reaching 8.6 km, for example, were located at the southern edges of the squall line. Cell I was still in its early development, not yet reaching 6 km. Nevertheless, hail was observed at 1630 MST when this cell passed over the northernmost pibal site.

At 1552 MST, a sounding was launched at the radar site. At this time, the leading cell I was 25 km north of the radar with the squall line well to the northwest. The hodograph shown in figure 3 indicates considerable wind shear in the lower levels up to about 10,000 ft. Above that level, the rate of increase of wind speed with height was considerably less. The echo motion, which represents the motion of the squall line as a whole and not the motion of individual cells, is seen to coincide with the winds at 10,000 ft.

All hail reports were received from an area to the north of the radar; the largest hail was described as walnut-size.

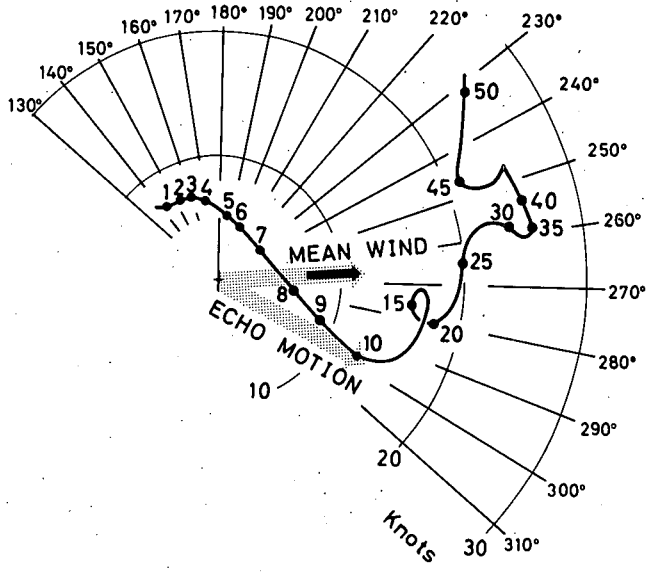

FIGURE 3.—Hodograph of environmental winds (kt) from radiosonde ascent at 1552 MST (ascent no. 1 in figs. 4–8). Mean wind is computed from the balloon position at approximate height of maximum observed radar top. Numbers indicate height (thousands of ft).

The Wind Field in the Horizontal

A detailed mesoscale analysis was performed in this case with good-quality data. During a period of more than 4 hr, 27 ascents were made from three stations with a separation of about 20 km (fig. 1). Most of the ascents reached 8,000 ft. Figures 4–8 present the horizontal patterns along with radar data obtained at 1755 MST just after a gust front passed over the three observation sites.

The 0/500-ft [2] winds relative to the storm display a well-organized mesoscale pattern (fig. 4A). A gust front has been indicated for this layer, although its exact position is known only at the southernmost pibal site where the time of passage was noted. Its extent toward the north was inferred from approximate times at the two other sites. The discontinuity was organized perpendicular to the direction of storm motion with the flow ahead of the gust front directed toward the echo, suggesting a region of confluence. In particular, the winds at ascents number 5 and 7 are blowing out of cell I with a component toward the right.[3] This part of the echo is, however, not representative of the time when cell I actually passed over the northernmost pibal site. Hail and rain were observed at 1630 MST, 10 min prior to the release of number 5, at which time the echo was already over and ahead of this site.

With the passage of the gust front, the wind shifted to a vigorous flow toward the right side of the storm and continued in that direction throughout the extent of the radar echo. Flow toward the left was found in the rear of the echo. The divergence pattern (fig. 4B) shows three distinct regions: convergence ahead of the echo, a 40-km wide area of divergence extending across the echo region, and slight convergence behind the echo. The pattern of vorticity is less well organized (fig. 4C). A maximun of cyclonic vorticity is centered along the gust front. The pattern of vertical velocity shows weak downward motions throughout the echo region (fig. 4D). The 500/1,000-ft layer (not shown) is similar except that wind speeds behind the discontinuity are stronger than in the lowest layer.

The 1,000/1,500-ft winds and divergence field show patterns similar to those in the lower layers (figs. 5A, 5B). The vorticity distribution (fig. 5C) is more clearly organized than in the lowest levels, with anticyclonic vorticity in the echo region and cyclonic vorticity ahead

[2] In the following, the layers will be designated by their lower and upper levels. The 1,500/2,000-ft layer, for example, refers to the layer between 1,500 and 2,000 ft.

[3] In the following, "right" and "left" will be used in the sense of an observer looking in the direction toward which the storm moves.

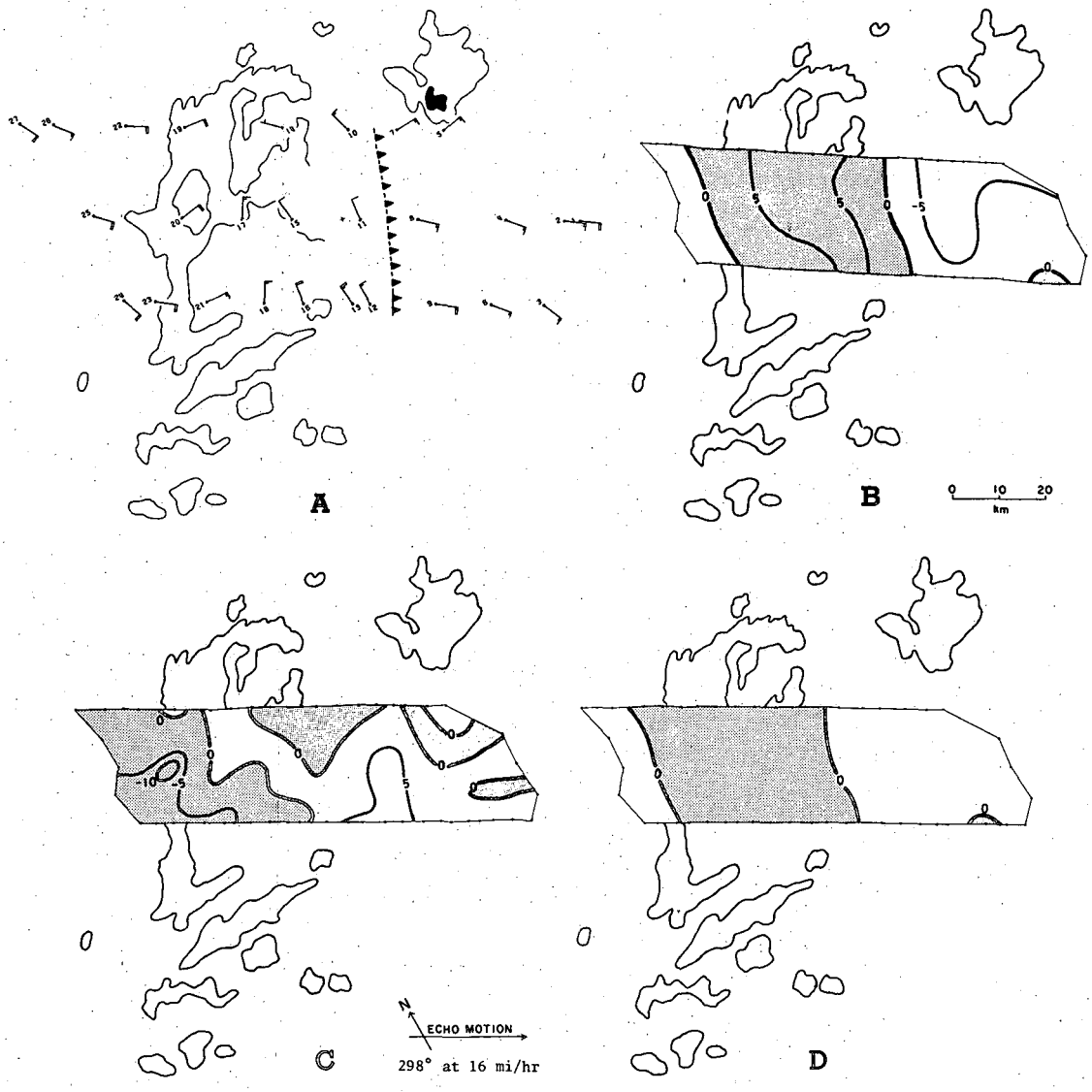

FIGURE 4.—The fields of (A) relative wind [true wind minus storm movement (kt)], (B) divergence [$10^{-4}s^{-1}$ (divergent where shaded)], (C) vorticity [$10^{-4}s^{-1}$ (anticyclonic where shaded)], and (D) vertical velocity [10 cm/s (downdraft where shaded)] for the 0/500-ft layer. Winds are plotted relative to the moving storm with the ascents numbered in their time sequence. Cross denotes position of radar at 1755 MST for which time the radar echoes are shown. Line with dots indicates outer boundary of data points.

of it. These areas match well with those of divergence and convergence. Thus, it appears that there is a preference for positive vorticity to be associated with convergence and negative vorticity with divergence, as one would expect on the large scale.

The layers between 1,500 and 4,000 ft (not shown) exhibit an organization similar to that in the layers below, but they show a decrease in the values of divergence and vorticity. Updrafts reach 1 m/s at 4,000 ft above the gust-front region.

The 4,000/6,000-ft winds indicate a sharp decrease in speed in the region above the surface discontinuity (fig. 6A). The stronger west winds are found farther back than in the lower levels; therefore, in relative motion, a flow from the east extends farther into the storm than at lower levels (cf. fig. 5A). This suggests a sloping of the gust front, and a diminishing of the strong gradients with increasing height. The divergence field (fig. 6B), showing mainly weak convergence, differs from that in the lower levels; the vorticity field, however, still displays a similar pattern (fig. 6C).

The 6,000/8,000-ft layer, for which fewer data are available, shows disorganized distributions of divergence and vorticity with slight convergence and anticyclonic vorticity throughout most of the region (figs. 7B, 7C). Vertical velocities (fig. 7D) indicate a downdraft region with maximum values around 1 m/s near the center of the echo system; the updraft speeds are still below 1 m/s.

Winds only are shown at the higher levels. The flow in the 8,000/10,000-ft layer (fig. 8A) suggests convergence within the echo region, with air streaming toward the storm from both directions.

The 10,000/12,000-ft winds (fig. 8B) still display strong flow toward the storm from the rear, with ascents number 13 and 21 indicating convergence. Winds ahead of the echo, however, appear to be weak.

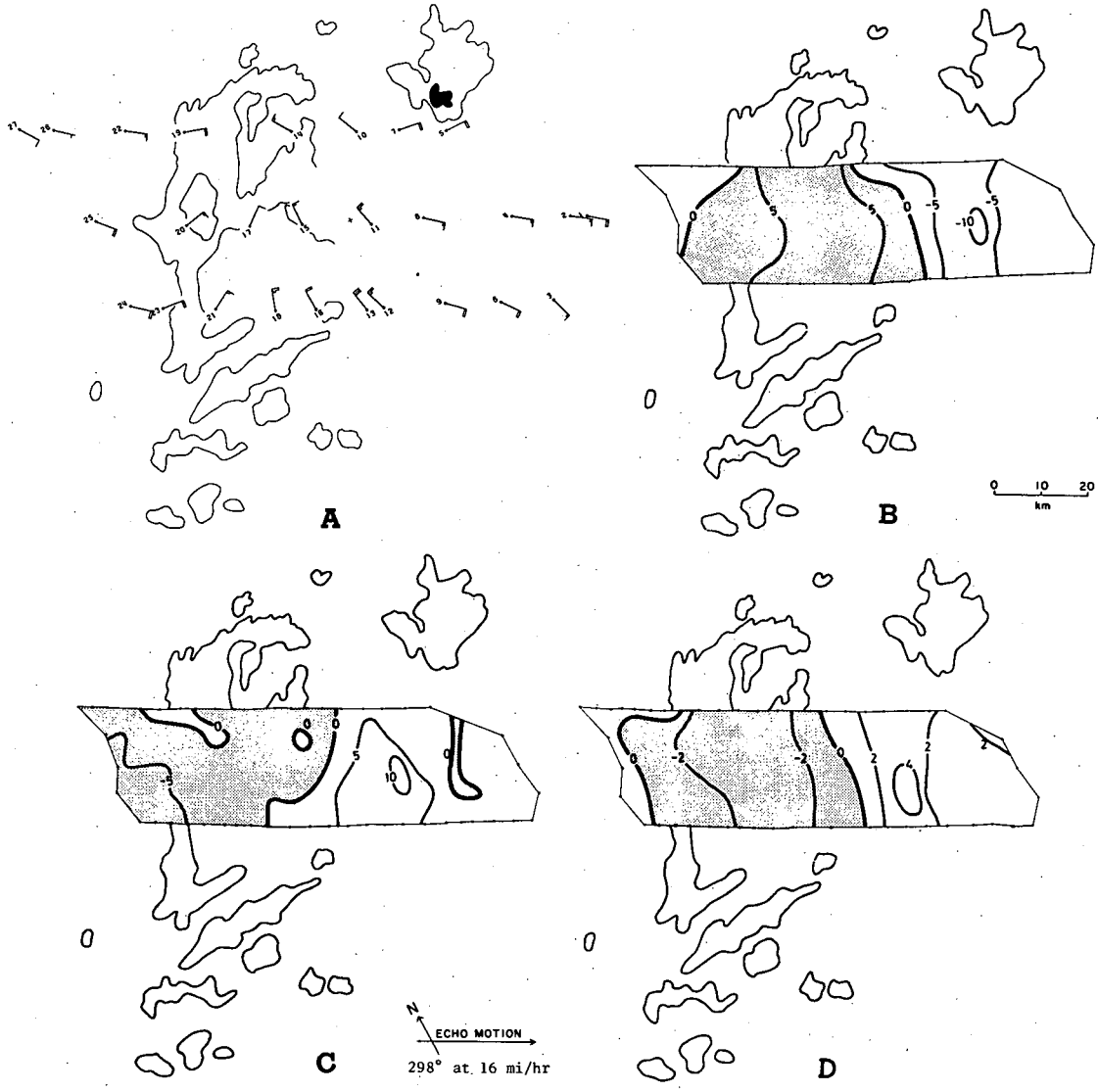

FIGURE 5.—Same as figure 4 for 1,000/1,500-ft layer.

The Wind Field in the Vertical

The airflow around the squall line exhibited some symmetry with respect to the direction of storm motion, with the gust front, in particular, oriented normal to this direction. It appears reasonable, therefore, to study the mean characteristics of the flow, averaged across the whole storm system and displayed in a vertical plane parallel to the direction of storm motion. Figure 9 presents vertical cross sections of these flow characteristics in the plane of storm motion, obtained by averaging along lines normal to the plane.[4] Horizontal distance is measured from the projection of the radar site at 1755 MST.

The horizontal wind component, u, parallel and relative to the moving storm (fig. 9A), clearly indicates the gust-front zone as a region of strong gradients, $\partial u/\partial x$ on its leading edge and $\partial u/\partial z$ on its upper slope. The normal component, v, displayed in figure 9B, also indicates strong shear in this region. A substantial portion of the airflow behind the discontinuity but in the leading part of the storm has a component away from the storm; that is, it is moving faster than the echo. The u maximum located in the center of figure 9A at about 1,000 ft is associated with an absolute maximum in v.

The divergence pattern (fig. 9C) shows a region of convergence centered around the gust front. A distinct core of low-level divergence is found behind the gust front at about 1,000 ft, with divergent flow extending up to 5,000 ft.

The vorticity distribution (fig. 9D) displays a center of cyclonic vorticity associated with the discontinuity in the wind field. In the levels below 5,000 ft, there appears to be a fair match between regions of positive vorticity and convergence and between negative vorticity and divergence. At higher levels where the divergence is weaker, no preference for such a relationship appears.

The vertical velocity field (fig. 9E) shows a downdraft area nearly 40-km wide with maximum downdrafts

[4] Because horizontal averaging was used in generating these cross sections, the different fields are not necessarily mutually consistent. For example, the region of rather strong (50 cm/s) updraft in the upper right portion of figure 9E cannot be explained by the relatively flat field of divergence shown in this part of figure 9C. The divergence cross section was obtained by averaging individual vertical profiles of divergence in the horizontal. The vertical velocity cross section was likewise obtained by averaging individual velocity profiles, *not* by integrating the horizontally averaged divergence field. Inconsistencies may then arise, especially at high altitudes (as in this example), where the number of vertical profiles used in calculating the horizontal averages begins to decrease.

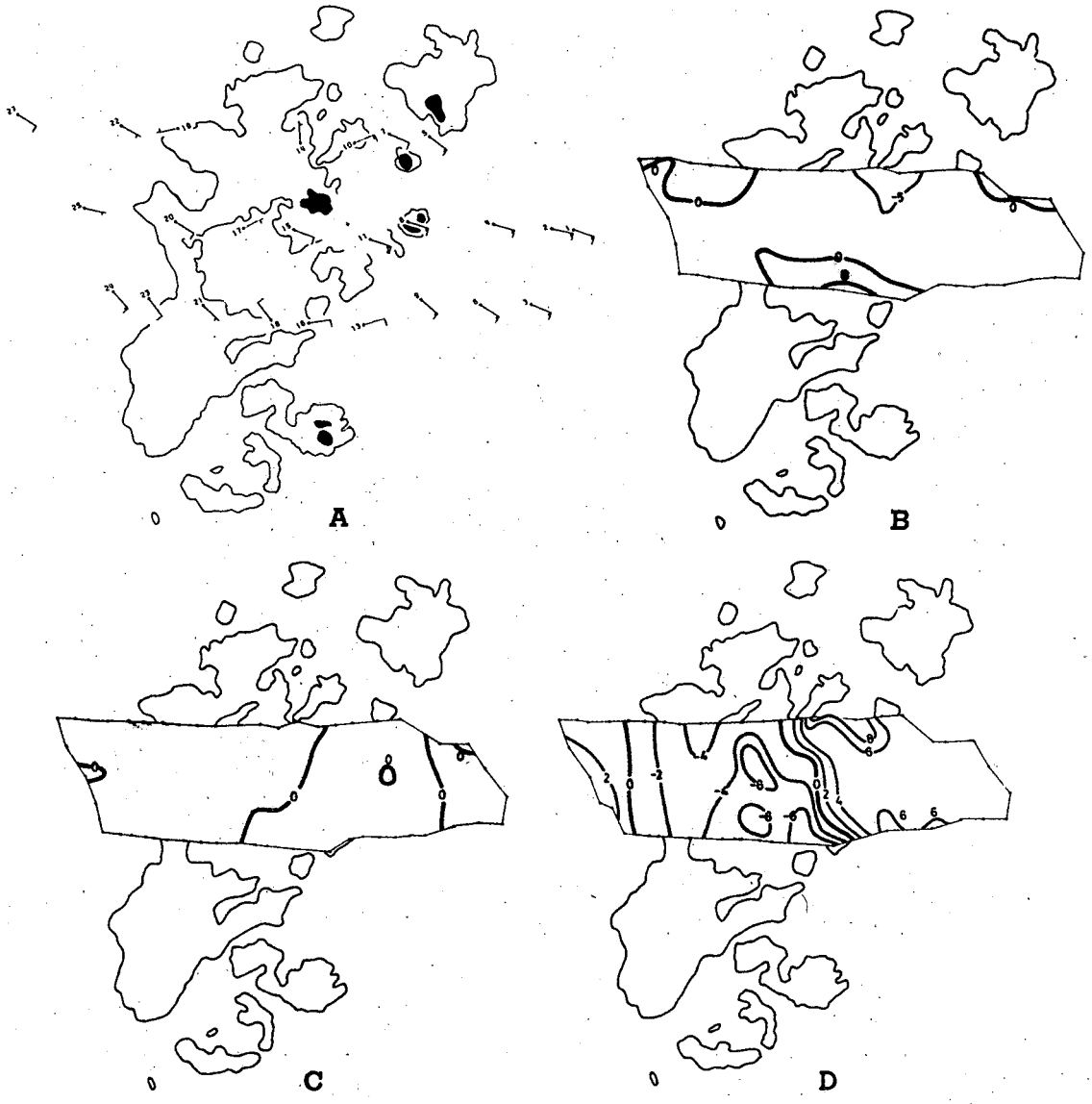

FIGURE 6.—Same as figure 4 for 4,000/6,000-ft layer.

occurring in its center and extending above the 9,000-ft level. Updrafts appear to be weaker; however, this is a result, in part, of the averaging process. A core of maximum upward motion is situated above the surface discontinuity.

Figure 10 shows the averaged flow relative to the surface; figure 11, the flow relative to the storm. In each case, the vectors were obtained by combining the fields of u and w. The pattern of the airflow relative to the moving echo (fig. 11) exhibits a simple structure. The picture is dominated by a vertically descending stream that draws in environmental air from the back of the storm at levels above 8,000 ft and from the front of the storm above 5,000 ft. This descending current spreads out symmetrically near the surface, forming a gust front on its leading edge. A vortex, centered between 3,000 and 4,000 ft occupies the transition zone between the downdraft and updraft regions above the gust front. Another vortex is found in the back of the downdraft core, formed by the outflow near the ground and the inflow above 8,000 ft.

In addition to the averaged fields, which are presented without radar information, vertical sections were prepared using specific selected triangles, formed by ascents taken at the radar site and the northern or southern pibal site, respectively (figs. 12, 13). For these, radar cross sections were constructed from the same PPIs used for the horizontal patterns of figures 4–8. The southern and the northern cross sections display similar features. The vertical velocities based on individual triangles yield values of greater magnitude than were found in the averaged cross sections. In particular, vertical velocities exceeding 1 m/s were observed within the updraft region in both cross sections at levels higher than 3,000 ft above the surface discontinuity. Downdrafts of 1 m/s were found in the southern cross section at levels higher than 6,000 ft.

Figure 14 summarizes the flow pattern in a true-scale diagram, with the northern radar cross section superimposed upon the relevant part of the radar echo projection of figure 2. The vertically oriented downdraft core is seen in the central portion of the echo projection, with the gust

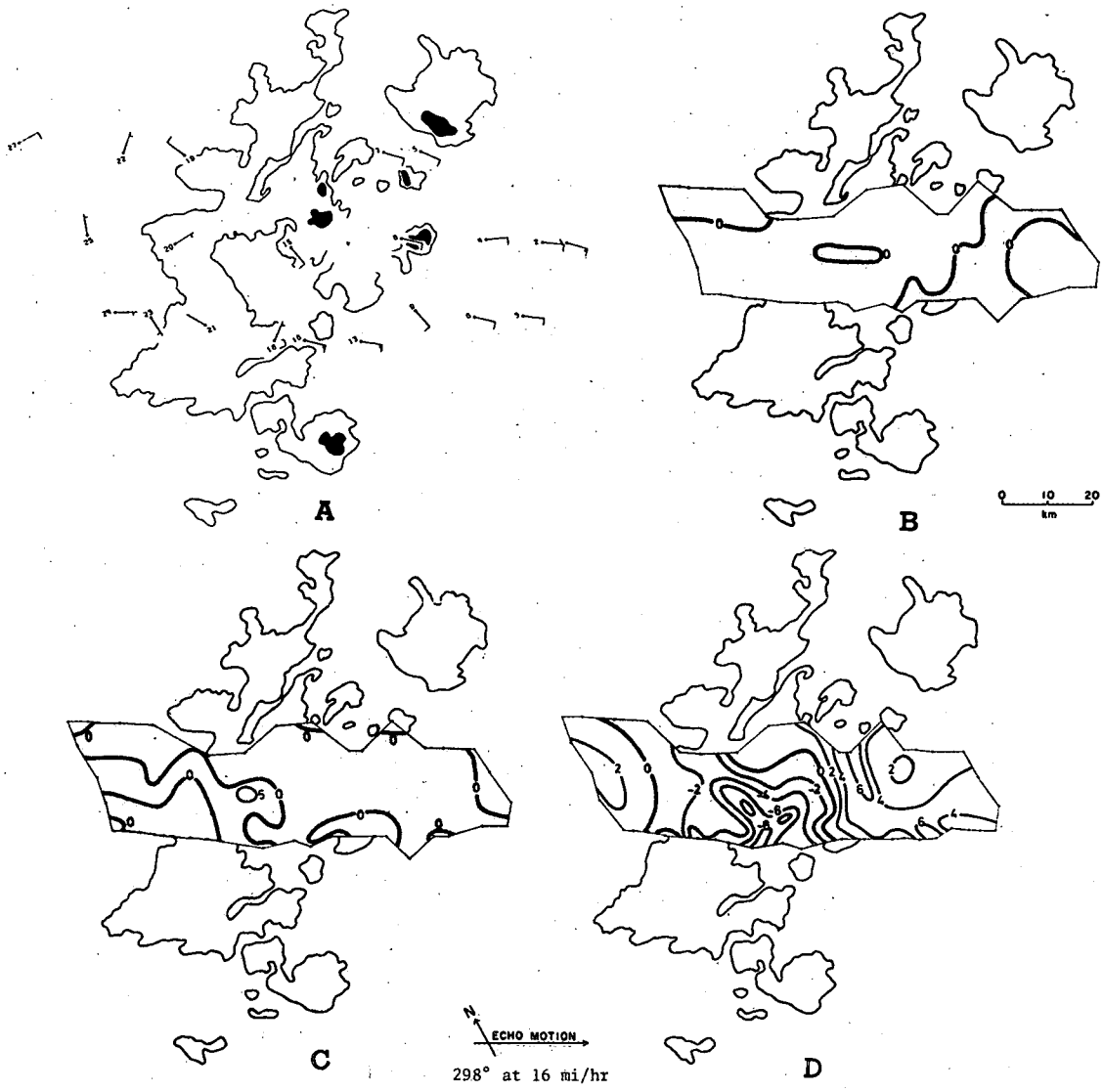

FIGURE 7.—Same as figure 4 for 6,000/8,000-ft layer.

front extending several kilometers ahead of the precipitation. The vortex above the discontinuity is located at the leading edge of the precipitation. Air is flowing into the squall line above this vortex with a mesoscale updraft area extending more than 25 km ahead of the gust front.

4. SUMMARY AND DISCUSSION

In the previous section, the analysis of one hailstorm was presented. We shall now summarize the results obtained from the analyses of all five storms and attempt to point out similarities as well as differences found in the mesoscale structure of these storms. Clearly, five cases form a very small sample that does not allow us to derive sweeping generalizations. Some of the results, however, may suggest the presence of common features. Since the radar echo was the key in directing mobile units into the vicinity of the storm, most observations were made near precipitation. As a consequence, the downdraft regions associated with the storm's precipitating part were better observed than the adjacent updraft regions. We will therefore discuss the downdraft areas and their accompanying divergence patterns first.

In all cases, downward motions existed throughout most of the echo region. For those cases in which the downdraft area extended into the rear of the echo, air trajectories in the downdraft core were directed toward the back of the storm—the core itself was located in the rear portion of the echo. In the one case (the storm of July 17, 1968) in which the downdraft area is known not to have extended into the rear of the storm, the core was situated in the central part of the echo with an air trajectory oriented normal to the direction of storm motion.

Divergence accompanying the mesoscale downdrafts in most cases reached up to 4,000 or 5,000 ft with a maximum located at about 1,000 ft. The vertical extent of the divergence region undoubtedly depends on the stage of the storm's development (Byers and Braham 1949). In a dissipating cell, for example, it reached beyond the 6000-ft level.

In four cases, including the storm of July 17, 1968,

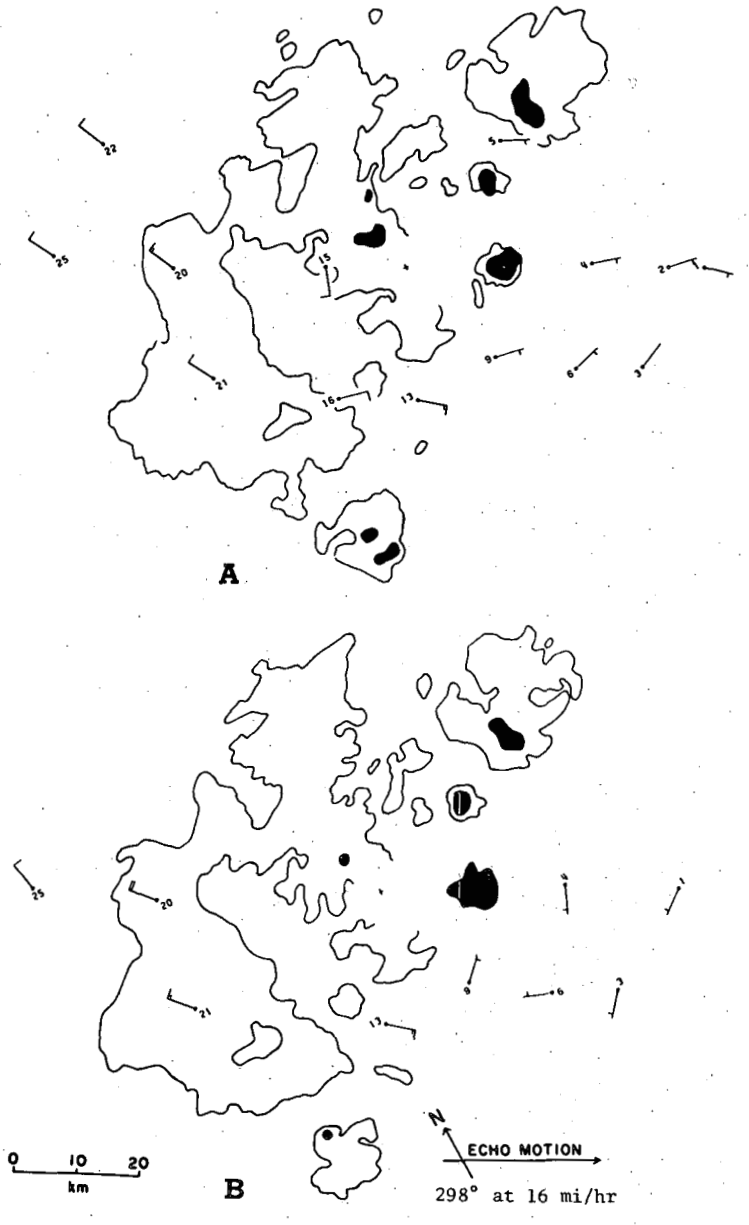

FIGURE 8.—Relative wind field (kt) for (A) 8,000/10,000-ft layer and (B) 10,000/12,000-ft layer.

the patterns of divergence and vorticity suggest that divergence is associated with anticyclonic vorticity. This relationship, which seems to be established only in the lower levels where the divergence is large (i.e., below 5,000 ft), appears to be associated with an advanced stage in the storm's lifetime. The accumulation of cold air in the lower levels probably induces a meso-High with a strongly divergent but anticyclonic circulation (Fujita 1955).

Let us now turn to the updraft areas. In summary, a mesoscale updraft region was found in front of the approaching storm in four cases. In three cases, including the storm of July 17, 1968, it extended to at least 25–30 km ahead of the echo. Intense updraft centers supplying the active cells of the storm systems were in most cases not observed. In a supercell-type storm (Browning and Donaldson 1963), an updraft maximum was found below an echo-free vault on the right side of the echo.

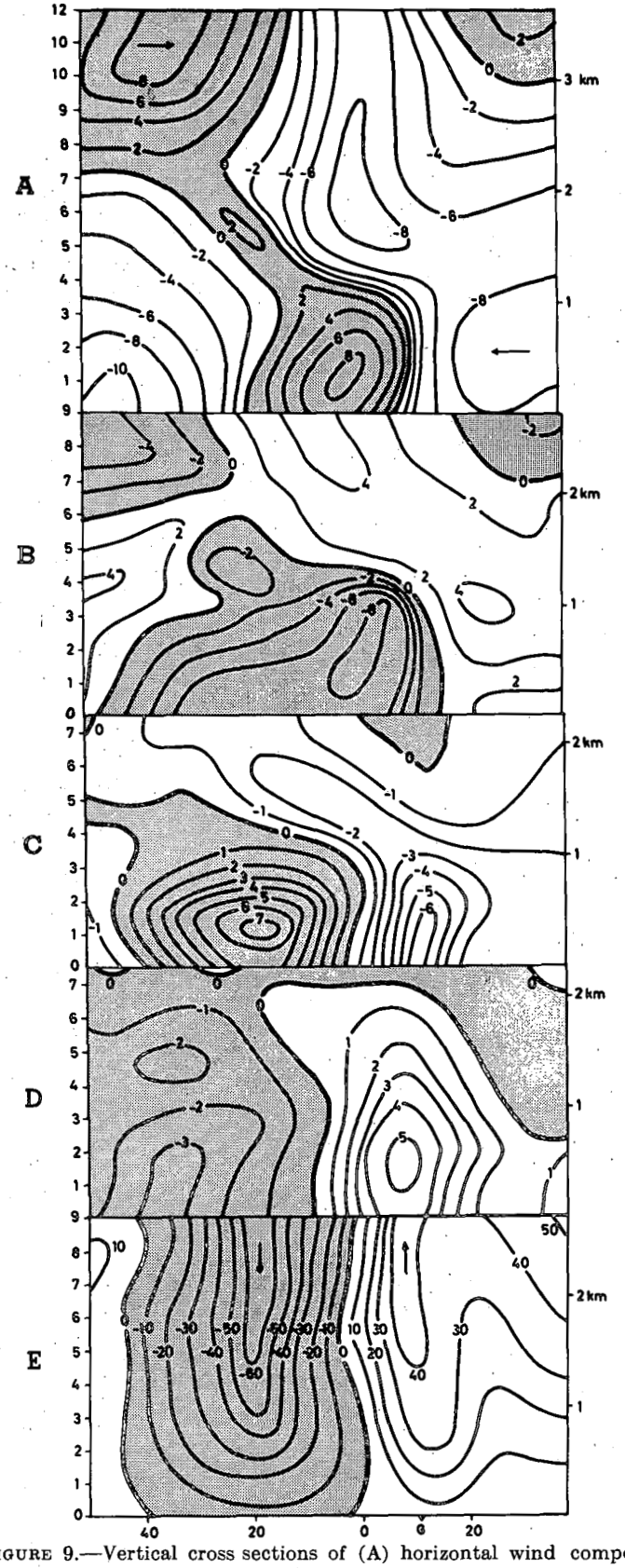

FIGURE 9.—Vertical cross sections of (A) horizontal wind component, u (m/s) relative to the storm in the plane of its motion (flow in the direction of storm motion where shaded), (B) horizontal wind component v (m/s) normal to direction of storm motion (flow toward the right side of the storm where shaded), (C) horizontal velocity divergence [$10^{-4}s^{-1}$ (divergent where shaded)], (D) vorticity [$10^{-4}s^{-1}$ (anticyclonic where shaded)], and (E) vertical wind component [cm/s (downdraft where shaded)]. G denotes the position of the gust front, and height scale on left is in thousands of feet.

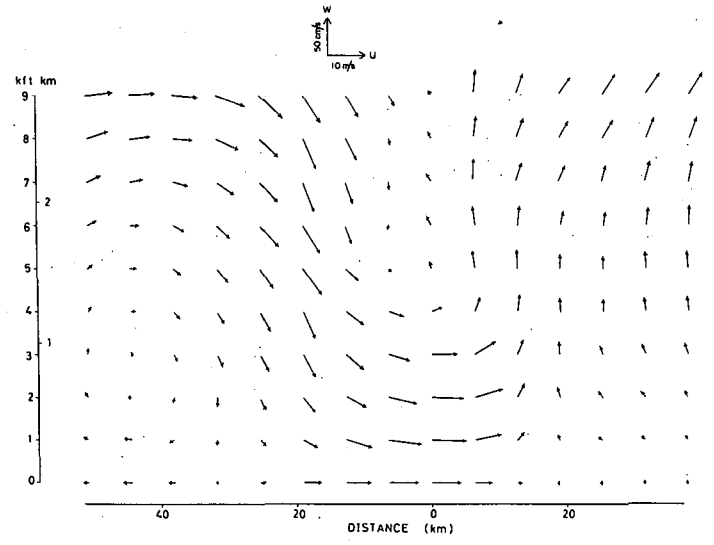

FIGURE 10.—Average flow relative to the surface in the plane of storm motion. Horizontal distance is measured from projection of radar site at 1755 MST.

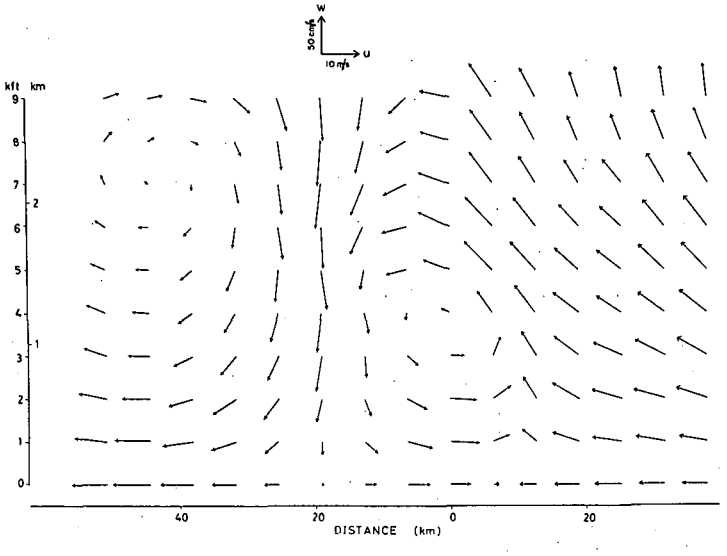

FIGURE 11.—Same as figure 10 for average flow relative to the storm.

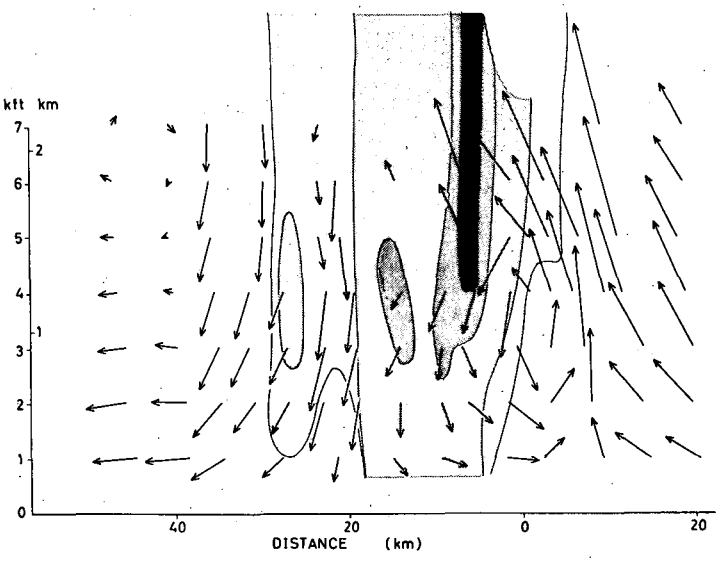

FIGURE 12.—Airflow relative to the storm in the plane of its motion. Wind vectors are obtained from selected ascents released at the two northern pibal sites. Radar cross section at 1755 MST in shades of gray is drawn halfway between the two sites.

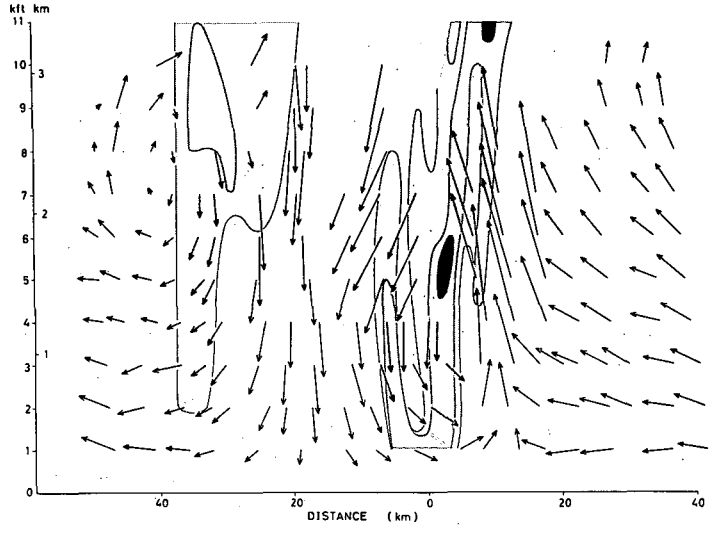

FIGURE 13.—Same as figure 12 for wind vectors obtained from selected ascents from two southern pibal sites.

In the cases where large gust fronts were observed ahead of the echo, regions of maximum upward motion were found either above the surface discontinuity (July 17, 1968, for example) or slightly ahead of the gust front. Weaker updrafts were observed downwind (with respect to the low-level winds) of the downdraft regions in three cases, including the storm of July 17, 1968. The convergence associated with low-level upward motion appears to have a relative maximum at about 1,000 ft. In the same three cases, convergence in front of the storm was associated with cyclonic vorticity, suggesting a relationship similar to that already discussed for divergence and anticyclonic vorticity. These three storms were accompanied by well-developed gust fronts in front of the echoes. However, two distinct gust-front organizations were observed.

On two occasions, including the storm of July 17, 1968, the leading edge of the discontinuity was found ahead of the precipitation, oriented normal to the direction of echo motion with the upper boundary of the gust front sloping back toward the echo. Surface winds in excess of the echo motion were observed behind it with a maximum occurring a few kilometers behind the discontinuity. A convergence maximum was centered at the gust front with convergence extending into the storm's outflow region, thus forcing air up near its leading edge. The squall line of July 17, 1968, is believed to have been in slow decay, while the other storm is known to have been dissipating rapidly.

On another occasion, however, precipitation was encountered prior to the gust front's passage. The surface discontinuity was not oriented normal to the direction of storm motion, and, in the vertical, the gust front appeared to have been tilted away from, rather than toward, the echo. Winds relative to the surface did not exceed the echo motion. A convergence maximum was located ahead of the gust front with convergence extending only a small distance behind it. Convection was still vigorous in this

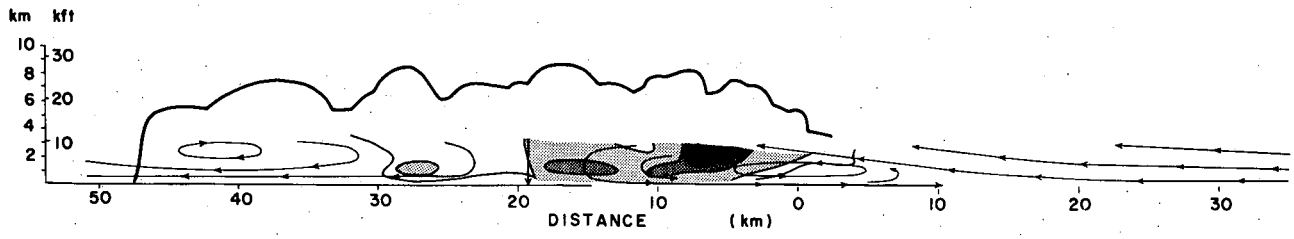

FIGURE 14.—True-scale view of the storm normal to its direction of motion. Outline of the radar echo projection at 1637 MST (fig. 2) is superimposed on the cross section at 1755 MST (fig. 12). Streamlines of flow are relative to the storm. Horizontal distance is measured from the projection of the radar site at 1755 MST.

case beyond the time at which the gust front was encountered. This organization is believed to have been associated with the early stage of the gust front's formation, while the previously described structure is thought to represent a more advanced state of its development.

A feature common to these three cases is the cyclonic shear accompanying the gust front. Winds were observed to shift with a flow toward the right side of the storm behind the gust front. Momentum conservation of descending air may explain this behavior in one case only. Apparently, the dynamic structure of the storm system is such as to induce these accelerations.

ACKNOWLEDGMENTS

The author wishes to express his sincerest appreciation to W. Hitschfeld and R. R. Rogers for their continued support and help throughout the course of this study. Thanks are also due N. H. Thyer, who made his computer programs available, and the staff of the Alberta Hail Studies project whose combined organizational effort in the data collection made this work possible. Financial support was provided by the Canadian Atmospheric Environment Service.

REFERENCES

Bellamy, John C., "Objective Calculations of Divergence, Vertical Velocity and Vorticity," *Bulletin of the American Meteorological Society*, Vol. 30, No. 2, Feb. **1949**, pp. 45–49.

Byers, Horace R., and Roscoe R. Braham, *The Thunderstorm*, U.S. Government Printing Office, Washington, D.C., June **1949**, 287 pp.

Browning, Keith A., and Robert J. Donaldson, Jr., "Airflow and Structure of a Tornadic Storm," *Journal of the Atmospheric Sciences*, Vol. 20, No. 6, Nov. **1963**, pp. 533–545.

Fujita, Tetsuya, "Results of Detailed Synoptic Studies of Squall Lines," *Tellus*, Vol. 7, No. 4, Stockholm, Sweden, Nov. **1955**, pp. 405–436.

Ragette, Gerd, "The Low Level Mesoscale Wind Field of Alberta Hailstorms," *Scientific Report* MW–69, Stormy Weather Group, McGill University, Montreal, Canada, Sept. **1971**, 51 pp.

Thyer, Norman H., "A New Method of Double Theodolite Pibal Evaluation," Alberta Hail Studies 1966, *Scientific Report* MW–49, Stormy Weather Group, McGill University, Montreal, Canada, May **1967**, pp. 1–26.

Thyer, Norman H., "Wind Measurements Near Alberta Hailstorms, 1966–67," *Scientific Report* MW–67, Stormy Weather Group, McGill University, Montreal, Canada, June **1970**, 28 pp.

[*Received November 19, 1971; revised August 11, 1972*]